NeuroImage: Clinical 21 (2019) 101633

Contents lists available at ScienceDirect

NeuroImage: Clinical

journal homepage: www.elsevier.com/locate/ynicl

Selective sensory deafferentation induces structural and functional brain plasticity

Raphael F. Casseb[a,b,1], Brunno M. de Campos[a], Alberto R.M. Martinez[a], Gabriela Castellano[b], Marcondes C. França Junior[a,*]

[a] Neuroimaging Laboratory, Department of Neurology, University of Campinas, Campinas, SP 13083-888, Brazil
[b] Neurophysics Group, Gleb Wataghin Physics Institute, University of Campinas, Campinas, SP 13083-859, Brazil

ARTICLE INFO

Keywords:
Sensory-motor integration
MRI
Sensory neuronopathy
Deafferentation
Plasticity

ABSTRACT

Sensory-motor integration models have been proposed aiming to explain how the brain uses sensory information to guide and check the planning and execution of movements. Sensory neuronopathy (SN) is a peculiar disease characterized by exclusive, severe and widespread sensory loss. It is a valuable condition to investigate how sensory deafferentation impacts brain organization. We thus recruited patients with clinical and electrophysiological criteria for SN to perform structural and functional MRI analyses. We investigated volumetric changes in gray matter (GM) using anatomical images; the microstructure of WM within segmented regions of interest (ROI), via diffusion images; and brain activation related to a finger tapping task. All significant results were related to the long disease duration subgroup of patients. Structural analysis showed hypertrophy of the caudate nucleus, whereas the diffusion study identified reduction of fractional anisotropy values in ROIs located around the thalamus and the striatum. We also found differences regarding finger-tapping activation in the posterior parietal regions and in the medial areas of the cerebellum. Our results stress the role of the caudate nucleus over the other basal ganglia in the sensory-motor integration models, and suggest an inhibitory function of a recently discovered tract between the thalamus and the striatum. Overall, our findings confirm plasticity in the adult brain and open new avenues to design neurorehabilitation strategies.

1. Introduction

In the last twenty years, studies have pointed to an underestimated role of the sensory system in the pathophysiology of movement disorders, such as Parkinson's disease (Patel et al., 2014b), dystonia (Patel et al., 2014a; Perruchoud et al., 2014) and Tourette's syndrome (Patel et al., 2014b). Compelling evidence like the alleviating maneuvers (Patel et al., 2014a) and the sensory cues (Patel et al., 2014b) may indicate, at least, a modulatory influence of the sensory inputs on movement disorders.

In this sense, an integrative model that considers an interplay between sensory and motor systems seems to be more adequate and even more helpful to elucidate the mechanisms of these conditions. We could assume, as a fundamental framework, a continuum of sensory-motor symptoms, pending between the sensory extreme (in traditionally sensory diseases) and the motor extreme (in the case of "purely" motor disorders). Broadly, this hypothesis states that both aspects would be affected in any condition, even if it is claimed purely sensory (or purely motor).

To the best of our knowledge the most recent discussions regarding sensory-motor integration were presented by Patel et al. (2014b) and Perruchoud et al. (2014). Both groups agree that proper sensory-motor integration is capital to adequate motor and sensory functioning. Patel et al. reviewed the sensory aspects of movement disorders, and addressed more specifically the structural organization of brain structures involved in this circuitry. Perruchoud et al., in turn, focused more on

Abbreviations: ANCOVA, analysis of covariance; DTI, diffusion tensor imaging; EPI, echo planar imaging; FA, fractional anisotropy; FDR, false discovery rate; FOV, field of view; FWE, family-wise error; GM, gray matter; MD, mean diffusivity; MRI, Magnetic Resonance Imaging; ROI, region of interest; SARA, *Scale for the assessment and rating of ataxia*; SN, sensory neuronopathy; T1WI, T1-weighted image; TE, echo time; TR, repetition time; WM, white matter

* Corresponding author at: Department of Neurology, University of Campinas – UNICAMP. Rua Tessália Vieira de Camargo, 126. Cidade Universitária "Zeferino Vaz", Campinas, SP 13083-887, Brasil.

E-mail addresses: brunno@fcm.unicamp.br (B.M. de Campos), gabriela@ifi.unicamp.br (G. Castellano), mcfrancajr@uol.com.br, mcfjr@unicamp.br (M.C. França Junior).

[1] Present address: Seaman Family MR Research Center, University of Calgary, Calgary, AB T2N 2T9, Canada.

https://doi.org/10.1016/j.nicl.2018.101633
Received 16 May 2018; Received in revised form 27 November 2018; Accepted 8 December 2018
Available online 11 December 2018

the functional perspective to detail how motor programs are informed and generated, and how these programs are monitored and subjected to correction.

In this scenario, sensory neuronopathies (SN) represent a unique human disease and may favor the investigation of sensory-motor integration, since the sensory and the motor domains are dissociated. SN comprises a rare subgroup of peripheral neuropathies characterized by restricted damage to dorsal root ganglia neurons. On clinical grounds, these patients have severe sensory deficits but preserved muscle strength. Afferent ataxia and incoordination are often found and represent the major source of disability.

There are very few MRI-based studies involving SN patients. We believe that a comprehensive neuroimaging investigation in a cohort of patients would provide valuable information on sensory-motor integration. Specifically, we hypothesize that (1) the cerebellum (which receives body proprioceptive input via the inferior cerebellar peduncle) and (2) the posterior parietal region (which communicates with the cerebellum and integrates visuospatial information) will be functionally affected. Abnormalities in the (3) basal ganglia and (4) pre-motor areas are also expected. To accomplish that, we recruited a representative group of SN patients and performed multimodal structural and functional MRI-based analyses to determine how sensory deafferentation modifies brain morphometry and functioning.

2. Materials and methods

2.1. Subjects

Thirty-six consecutive SN patients, and 39 healthy volunteers were recruited between 2013 and 2016 at our University Hospital. Included patients met clinical and electrophysiological criteria, and the details of diagnosis are described elsewhere (Camdessanché et al., 2009). Nine SN patients were excluded because they presented incidental lesions ($n = 1$), neurological comorbidities ($n = 2$), neuroimaging artifacts ($n = 4$) or incomplete acquisition of MRI data (n = 2). At the time of MRI scanning and clinical evaluation, patients were being treated with the following medications: azathioprine ($n = 11$), azathioprine and steroids ($n = 2$), azathioprine and intravenous immune globulin ($n = 1$), azathioprine and mycophenolate ($n = 1$), methotrexate ($n = 1$), mycophenolate ($n = 1$), steroids ($n = 1$). Nine patients were not under any drug treatment for SN.

Twenty-seven healthy subjects (17 women; 51 ± 11 years old; age range: 26–77 years) and 27 SN patients (17 women; 51 ± 11 years old; age range: 26–75 years) were included in the analysis of GM and WM. A subgroup of 19 SN patients with longer disease duration (≥4 years; 13 women; 54 ± 10 years old; age range: 39–75) also underwent functional analyses. As only seven out of the 27 healthy volunteers had complete functional acquisitions, we recruited 12 additional participants to make up the control group of the functional analysis, comprising 19 healthy volunteers (14 women; 46 ± 12 years old; age range: 28–65 years).

This study was approved by our Ethics Committee and all participants that agreed to take part in the study signed an informed consent.

2.2. Clinical evaluation

Scale for the assessment and rating of ataxia (SARA) (Schmitz-Hübsch et al., 2006) was employed to evaluate disease severity since there is no specific scale to evaluate SN manifestations, and ataxia is the most similar clinical syndrome. Four patients were lost to follow up, hence our clinical dataset comprises only 23 patients.

2.3. MRI acquisition

All brain scans were performed in a 3T Philips Achieva scanner (Philips Healthcare, Best, The Netherlands) using an 8-channel head coil.

Structural images were acquired using a sagittal high-resolution T1-weighted image (T1WI) protocol, with isotropic voxels of 1 mm^3, no gap, flip angle = 8°, repetition time (TR)/echo time (TE) = 7/3.2 ms and field of view (FOV) = 240 × 240 mm^2.

Diffusion tensor images (DTI) were estimated from diffusion weighted images acquired with a spin echo single shot echo-planar imaging (EPI) sequence, with acquired voxel = 2 × 2 × 2 mm^3, reconstructed voxel = 1 × 1 × 2 mm^3, no gap, flip angle = 90°, TR/TE = 8500/61 ms, 70 slices, 32 gradient directions, maximum b-factor = 1000 s/mm^2 and FOV = 240 × 240 mm^2.

During the performance of a finger-tapping task, functional images were acquired using an axial T2*-weighted EPI protocol, with voxel size = 3 × 3 × 3 mm^3, gap = 0.6 mm, flip angle = 90°, TR/TE = 2000/30 ms, 40 slices, FOV = 240 × 240 mm^2, 110 volumes. Subjects were requested to perform a right-hand finger-tapping paradigm, comprised of six resting blocks of 22 s each,[2] alternated with five task blocks of 18 s each. A sound instruction indicated the beginning ("Start") and the end ("Stop") of movement execution for each task block. Subjects wore an electronic glove to monitor tapping frequency. Task session was performed twice: with eyes closed (non-visually guided) and with eyes open starring at the tapping fingers (visually guided).

2.4. MRI analyses

2.4.1. Structural analyses

2.4.1.1. Gray matter analysis. We used a platform available online (https://mricloud.org/) (Mori et al., 2016) to preprocess and segment structural T1WI (Tang et al., 2013; Wang et al., 2013). Images were first converted from DICOM to Analyze format using the Dcm2Analyze software for Windows (version 3), also available at https://mricloud.org/t1batch. Then, images were uploaded in the platform for preprocessing and ROI segmentation. Preprocessing was composed of: reorientation from sagittal to axial, which is the orientation of the platform atlases; inhomogeneities correction (Tustison et al., 2010); brain extraction (Tang et al., 2015); co-registration with some of the 45 adult labeled atlases (adult atlas version 9B – 26 atlases used if the participant age was in the range 22–50 years; or 19 atlases for the age range of 50–90 years); fusion of these co-registered labeled images for each participant (Wang et al., 2013). The resulting ROI-labeled image comprised 283 segmented brain regions in the native space of every subject. Twelve of them (six bilateral structures) were selected for between-group comparison based on our hypothesis, namely: caudate, cerebellum, globus pallidus, putamen, superior parietal lobule and thalamus. Volumes were obtained from the fifth ontology level of the type II hierarchical segmentation of the brain (Wu et al., 2016).

2.4.1.2. White matter analysis. WM microstructure was also assessed with the multi-atlas approach in the same online platform (https://mricloud.org/) (Li et al., 2013; Tang et al., 2013; Mori et al., 2016). Initially DICOM images were converted to a data parameter (*.dpf) and raw image (*.raw) files, with the software DwiDcm2DpfRaw for Windows available at https://mricloud.org/dtical. Preprocessing steps were: co-registration of diffusion weighted images to the b = 0 image using Automated Image Registration (Woods et al., 1998) to correct for eddy currents (Zhuang et al., 2006) and subject motion; diffusion tensor fitting; DTI parameters calculation (eigenvectors, eigenvalues and the derived fractional anisotropy – FA and mean diffusivity – MD); non-linear registration using a large deformation diffeomorphic metric mapping (Tang et al., 2014); and, finally, the segmentation (labeling) of brain regions based on FA, MD and eigenvectors of every voxel via a diffeomorphic likelihood fusion algorithm (Tang et al., 2014). Using the

[2] Except for the last resting block, that lasted 20 s.

labeled images and the FA maps, we were able to calculate the average FA value within each of the ROIs, and eventually carry out the between-groups comparisons.

As WM tracts of the selected brain structures are not fully described and elucidated, we preferred to perform the WM analysis in an exploratory fashion, thus not restricting the investigation to any particular tracts.

2.4.2. Functional analysis (finger-tapping task)

To preprocess functional images, we employed the UF^{2}C toolbox (version 7.1, https://www.lniunicamp.com/uf2c) (de Campos et al., 2016), which relies upon SPM12 (version 6685, Wellcome Trust Center for Neuroimaging, London, United Kingdom, http://www.fil.ion.ucl.ac.uk/spm, RRID: SCR_007037) and runs within Matlab (version 9.1, The MathWorks, Inc., Natick, Massachusetts, United States, RRID:SCR_001622). Dummy scans were used at the beginning of the acquisition to reach steady state, and a total of 110 volumes were collected. All structural and functional images were first reoriented in SPM12 to set the anterior commissure as the origin of the image space. Each functional dataset was then realigned to the first volume using a rigid body transformation, and the structural T1WI was co-registered to the mean functional image. Next, the segmentation step (Ashburner and Friston, 2005) was performed on the T1WI yielding the deformation parameters used for the normalization of structural and functional images into the MNI standard space. Finally, functional images were smoothed with a Gaussian kernel (FWHM = 6 × 6 × 6 mm^3).

Individual activation analysis (first level) was automatically performed by UF^{2}C, using ten regressors in the design matrix: the task paradigm convolved with the hemodynamic response function (1) + time and dispersion derivatives (2) + movement parameters of translation and rotation (6) + a constant value to account for the average of the signal (1). The resulting contrast images were used to compare activations within each group considering the two conditions (eyes open and eyes closed).

2.5. Experimental design and statistical analysis

Based on previous clinical and immunological data, patients were divided into long (n = 19) and short (n = 8) disease duration subgroups (Horta et al., 2011) to gather a more homogeneous cohort of subjects, using a duration cut-off of 4 years to define the subgroups. Volumetric analysis was conducted using a multiple analysis of covariance (ANCOVA) in SPSS (version 22, IBM Corp. Released 2013. IBM SPSS Statistics for Windows, Armonk, United States: IBM Corp, RRID: SCR_002865), with ROI volumes (in mm^3) as dependent variables and group as an independent variable. Age, sex and total brain volume were included as covariates in our model, and p values were corrected for multiple comparisons in Matlab. We employed the Benjamini and Hochberg correction (Benjamini and Hochberg, 1995) for the false discovery rate (FDR) at a significance level of 0.05 (*mafdr* Matlab function, using the linear step up procedure).

FA values from the DTI analysis were also compared between groups using a multiple ANCOVA model in SPSS, taking age and sex as covariates. FA average values within each ROI were the dependent variables, and group and covariates were the independent ones. P-values were FDR-corrected as well.

Pearson correlation coefficient was used to assess any linear relationship between the clinical scale (SARA) and structural measures (ROI volumes and FA values). Only regions that presented significant alterations in comparison to healthy controls were considered for correlation analysis.

Regarding finger-tapping activation assessment, every participant was assessed for the individual differences between eyes-open and eyes-closed condition, by contrasting the beta values for each condition. Resulting contrast images were then smoothed (FWHM = 6 × 6 × 6 mm^3; Gaussian kernel) and used for within-group comparison (second level) via a paired t-test in SPM12. Differences concerning eyes-open and eyes-closed conditions were FWE-corrected for multiple comparisons at the cluster level with $\alpha = 0.05$, to avoid the inflation of false positives as reported in (Eklund et al., 2016). Defining-cluster threshold was set to 0.001.

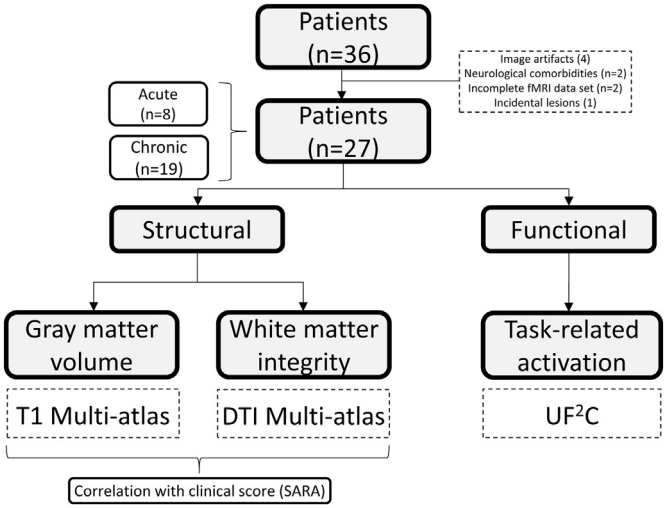

Fig. 1. Study Design. Scheme representing the rationale of the analyses performed and the tools used.

Fig. 1 summarizes the study design and the methods employed.

3. Results

3.1. Demographics

Clinical and demographic data of subjects are detailed in Table 1.

3.2. Structural results

3.2.1. Gray matter

The multiple ANCOVA revealed hypertrophy of the left caudate nucleus in the long disease duration group (p = 0.012, FDR-corrected) and a trend towards significance of the right caudate (p = 0.054, FDR-corrected) (Fig. 2). No differences were found in the short disease duration group (p > 0.05, FDR-corrected).

There was no correlation between caudate volumes and SARA

Table 1
Clinical and demographic data of SN patients

	Total SN (n = 27)	Long disease duration SN (n = 19)	Short disease duration SN (n = 8)
Age (mean ± SD, years)	51 ± 11	54 ± 10	42 ± 11
Gender (M/F)	10/17	6/13	4/4
Disease duration (mean ± SD, years)	10.4 ± 8.8	14.0 ± 8.1	2.6 ± 1.8
SARA (mean ± SD)	11.5 ± 6.0	13.2 ± 6.0	7.4 ± 4.1
Pseudoathetosis (%)	74	65	100
Disease course (%) (Acute/Subacute/ Chronic)	18/11/70	21/5/74	13/25/62
Etiology			
Idiopathic	15/27	11/19	4/8
Sjögren Syndrome	6/27	4/19	2/8
Autoim. Hepatitis	4/27	2/19	2/8
HTLV[a]	1/27	1/19	
MGUS[b]	1/27	1/19	

[a] Human T-cell lymphotrophic virus.
[b] Monoclonal gammopathy of unknown significance.

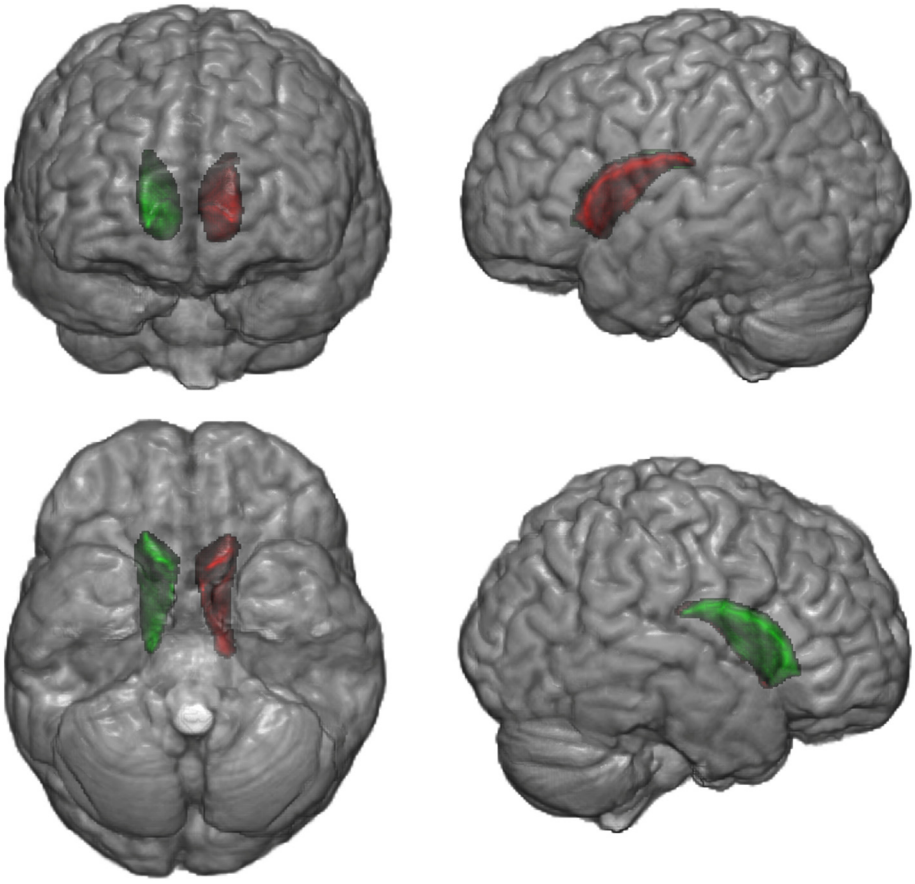

Fig. 2. Hypertrophic regions in the long disease duration subgroup of sensory neuronopathy (SN) patients. Gray matter volumetric analysis revealed hypertrophy in the left caudate nucleus of long disease duration subgroup compared to controls (FDR-corrected $p = 0.012$), and a trend towards significance of the right caudate (FDR-corrected $p = 0.054$). Green and red indicate the right and left caudate nuclei, respectively.

scores.

3.2.2. White satter

The analysis of DTI parameters, obtained with the multi-atlas segmentation approach, showed mean FA reduction in ROIs close to the thalamus and the striatum, namely: left and right anterior limbs of the internal capsule ($p = 0.029$ and $p = 0.029$), right anterior corona radiata ($p = 0.034$), right external capsule ($p = 0.029$), right posterior corona radiata ($p = 0.048$), right posterior thalamic radiation ($p = 0.029$), right superior longitudinal fasciculus ($p = 0.029$), left body of corpus callosum (0.029), left fornix (0.029) and left superior corona radiata ($p = 0.048$) (Fig. 3). (All *p*-values are FDR-corrected).

We also calculated the Pearson correlation coefficient (r) between SARA scores and structural measures considering all the patients that were clinically evaluated ($n_{SARA} = 23$). Significant correlation values (uncorrected for multiple comparisons) were found between SARA and FA values for: the body of the corpus callosum ($r = -0.48$, $p = 0.02$), left fornix ($r = -0.48$, $p = 0.02$) and right posterior thalamic radiation ($r = -0.53$, $p = 0.01$). Linear regression plots are presented in Fig. 4. No significant correlations were found between SARA and caudate nuclei.

3.3. Functional results

We restricted our functional analyses to the healthy individuals and the long disease duration subgroup of SN patients, since structural abnormalities were not identified in the short disease duration subgroup.

3.3.1. Motor task (finger-tapping)

All participants were right-handed, and finger-tapping was executed only with the right hand. Performance of both groups (SN patients and controls) in terms of tapping frequency was similar during the task ($p > 0.05$ for both conditions).

We compared each group to assess differences between eyes-open and eyes-closed conditions. In the control group we noticed that occipital, parietal and cerebellar (lobes VI and VIII) regions were more active when eyes were open watching the fingers tapping (Fig. 5A). In the long disease duration group, however, only occipital regions were more active (Fig. 5B).

4. Discussion

As far as we know, not many studies on cases of sensory deprivation were published in the literature. We found, for instance, investigations regarding amputation (Makin et al., 2015; Raffin et al., 2016), blindness (Voss and Zatorre, 2015; Araneda et al., 2016) and spinal cord injury (Endo et al., 2007; Choe et al., 2013). From our perspective, we understand that blindness investigations are more interesting, because in the case of amputation and spinal cord injury there is – in general – a concomitant deprivation of both the input of sensory information and the output of motor commands, and therefore the patient is affected at both ends (sensory and motor). Yet, it is worth emphasizing that different phases in life of visual deprivation affect the functional reorganization in very different ways; see for example the marked peculiarities in cases of reorganization and re-adaptation following cataract surgery in early childhood (Lewis and Maurer, 2005) and in adulthood (Martins Rosa et al., 2013). Thus, it appears that the disease with the greatest dissociation between sensory and motor aspects in a mature brain is SN. Hence, this study aimed to investigate the impact of SN in the cerebral structures and the possible functional reorganization of the brain in such condition.

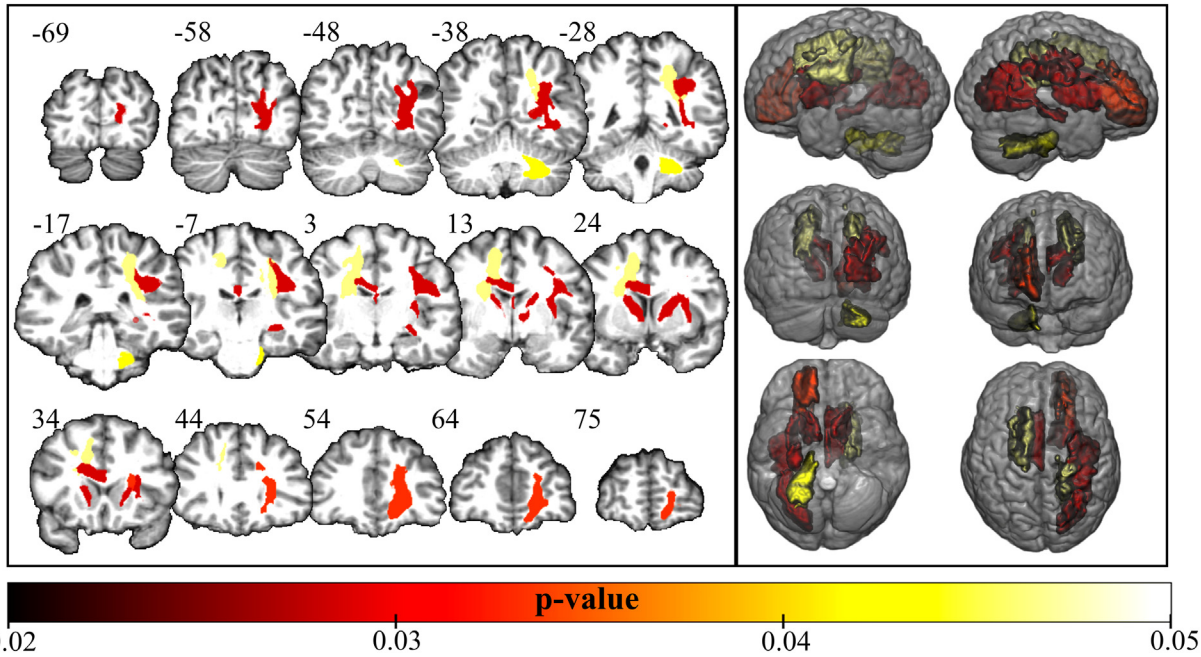

Fig. 3. White matter abnormalities in the long disease duration subgroup of sensory neuronopathy (SN) patients. Tracts with reduced mean FA values ($p < 0.05$ corrected for false discovery rate) in long disease duration subgroup of SN patients compared to controls. Numbers next to the coronal slices represents y coordinates (mm) in the MNI space. Even though the analysis was performed in the native space, the figure above was normalized to the standard MNI152 space for illustration purposes.

4.1. Structural gray matter findings

Considering that the basal ganglia are strongly involved in the motor circuitry, and that movement disorders are normally related to these structures, we decided to restrict our investigation to the basal ganglia and to additional regions implicated in the sensory-motor integration. Therefore, using a ROI-based method, we targeted the caudate nuclei, the putamen, the globus pallidus, the thalamus, the superior parietal lobule and the cerebellum.

Recent initiatives have released multi-atlas pipelines to segment brain structures and they have shown better performance (Tang et al., 2015) over traditional one-template methods (e.g.: FreeSurfer (Fischl, 2012)). With this approach, we found a significant increase in the volume of the caudate nuclei (a trend, in the case of the right caudate). Although counterintuitive, one should recall that axonal damage in some tracts may cause downstream hypertrophic abnormalities. For instance, this has been reported in hypertrophic olivary degeneration (Goyal et al., 2000) that follows damage to fibers within the Guillain-Mollaret triangle (red, inferior olivary and contralateral dentate nuclei).

In the SN case, the structural degeneration is believed to reach the sensory nuclei in the medulla, given the hyperintense T2 signal already described by some authors (Okumura et al., 1992; Casseb et al., 2015). However, there is no evidence to support direct effects on the basal ganglia. Curiously, caudate hypertrophy may suggest that at least a functional disturbance is perceived in the basal ganglia circuitry, which could raise two possibilities: that a structural connection link the medulla and the basal ganglia, or the presence of a diaschisis.

The caudate volume increase, in turn, is probably related to the lack of proprioceptive and vibratory inputs. Due to the fact that the alteration is only found in the long disease duration subgroup of SN patients (disease duration ≥ 4 years), we believe that it is a compensatory mechanism and not a direct effect of damage at the dorsal root ganglia.

Such hypertrophy could be related to overactive caudate nuclei, attempting to compensate the lack of sensory input with, perhaps, visual information. However, this compensation might be maladaptive, associated with loss of inhibitory input from other regions, as it is seen in Parkinson's disease.

Taking the model proposed by Patel et al. (Patel et al., 2014b) into account, we could hypothesize that the newly recognized tract between the thalamus and the striatum would be an inhibitory connection, with reduced activity due to loss of sensory input to the thalamus. Therefore, it could lead to a pathological overactivation of the caudate nuclei and hence, its increase in volume.

Regarding tissue hypertrophy, based on animal model studies (Raisman, 1969; Cotman et al., 1973), we hypothesized that this could be due to an eventual increase in neuropil and dendritic ramifications. Cotman et al. (1973), for example, showed that ablation of the entorhinal cortex produced a surprising increase of synaptic terminals in the target region in the animal model. Hence, a similar phenomenon could be taking place in patients with long disease duration. Recently, some signaling pathways involved with these histological changes have been investigated. Endo et al. (2007) identified alterations in the gene expression in the somatosensory cortex of rats submitted to spinal cord transection, which is another experimental model of deafferentation. There was a reduced expression of the Nogo receptor (*NgR*) and *LINGO-1* genes, and paradoxically, an increase in BDNF expression. Interestingly, changes in gene expression were temporally related to the change in the fMRI activation maps used to monitor cortical reorganization.

4.2. Structural white matter findings and correlation with clinical scales

DTI-based analysis is sensitive to detect WM abnormalities, including subtle microstructural changes. With the multi-atlas approach, we were able to show reduced FA in deep cerebral WM tracts connecting the basal ganglia, thalamus and cortical regions. These findings, combined with gray matter results, indicate that sensory deafferentation deeply impacts basal ganglia circuitry.

Moreover, three WM regions were correlated with SARA scores: the left body of the corpus callosum, the left fornix and the right posterior thalamic radiation. Corpus callosum and fornix are the major interhemispheric communication bundles. As FA reduction in these regions was negatively correlated with the SARA scores, we may infer that severity is somehow related to loss of connection between hemispheres. Coordination of movements that involve bilateral limb activation, such

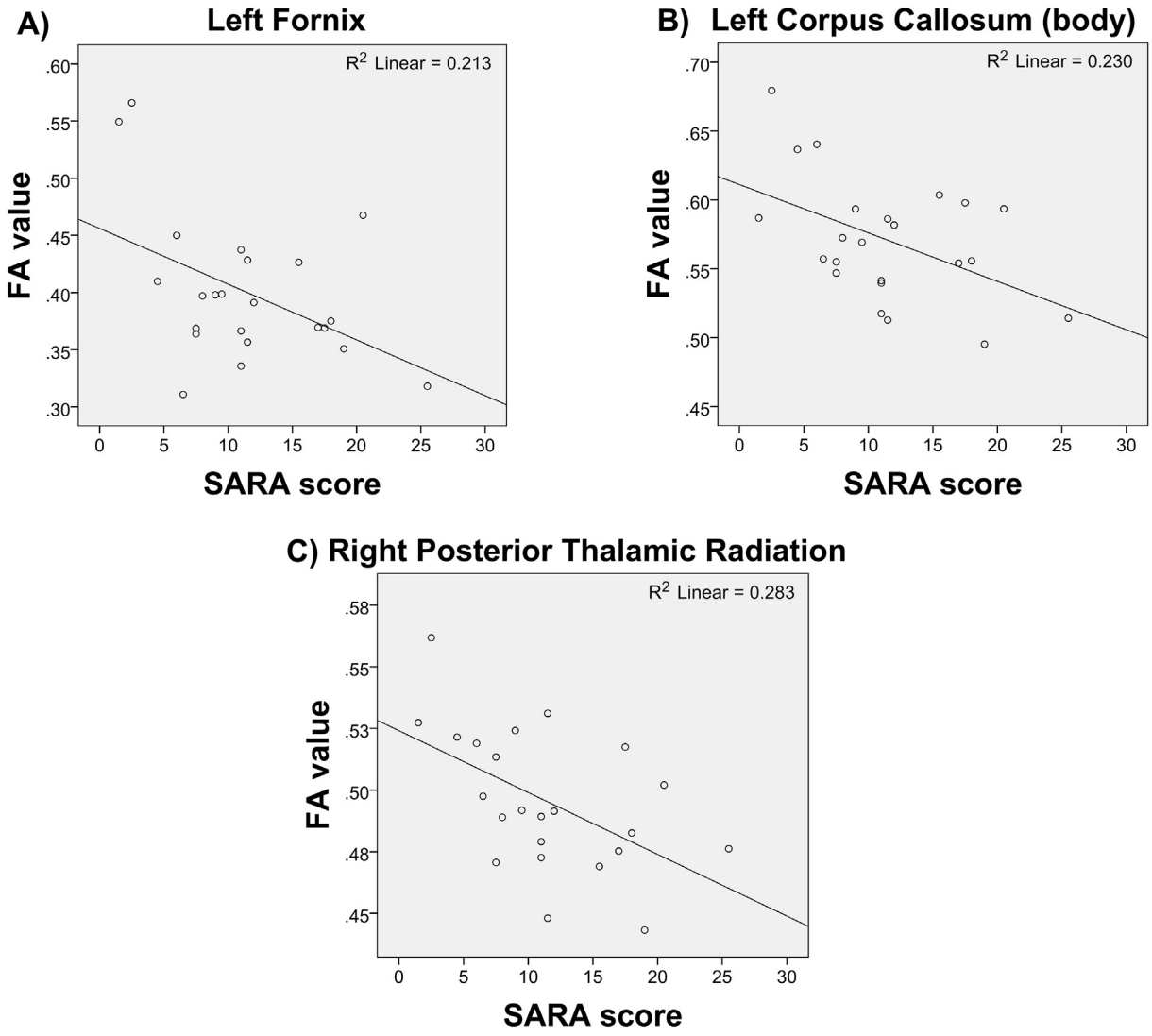

Fig. 4. Scatter plots showing the correlations between FA values and SARA scores. (A) Left fornix (LF), (B) body of corpus callosum (BCC), and (C) right posterior thalamic radiation (RPTR). Only regions of interest that showed significant association are depicted.

as gait, is deeply impacted by callosal damage (Gooijers and Swinnen, 2014). So, it is possible that gait ataxia found in SN patients is related to loss of interhemispheric connection.

Damage to commissural tracts measured via DTI parameters has also been reported in other conditions similar, in terms of deafferentation, to SN. Simoes et al. (2012) showed a consistent reduction of FA values in the body of the corpus callosum in a group of amputees. Rezende et al. (2016) found that FA values indicated a progressive microstructural degeneration of the corpus callosum, superior cerebellar peduncles and pyramidal tracts in a group of patients with Friedereich's ataxia. Interestingly, Friedereich's ataxia is the movement disorder that most closely resembles the clinical aspects of SN, although its pathophysiology relies ultimately on genetic alterations. Both examples illustrate that deafferentation may yield deficits in interhemispheric communication, and could be the basis of the correlation found between severity and FA measures in SN. To test this hypothesis, future studies could include bimanual tasks to investigate the synchrony in the motor performance of SN patients, and verify whether this relationship indeed exists.

We finally highlight that these results regarding correlation should be appreciated with caution, since they were not corrected for multiple comparisons. Therefore, we believe that our exploratory correlational analysis may serve as additional and speculative information, but should not be used alone to base other investigations.

4.3. Functional analyses findings (task-related activations)

Considering finger-tapping related activation with and without visual input, we found a greater area of activation among controls in the posterior parietal regions and in medial areas of the cerebellum in the former condition. These regions appear to be involved in the integration of proprioceptive and visual information. Interestingly, such pattern of activation is not found in the SN group, which means that functional behavior of the SN patient's brain is not changing from one condition to the other. If we consider that the posterior parietal cortex is related to the **integration** of sensory (proprioceptive) and visual inputs, we may speculate that the absence of proprioceptive information refrains the integration process, and therefore, the visual input would trigger no activation of the posterior parietal area. Visual information could, for instance, serve as a substrate to motor planning in a more direct way through the fronto-occipital fasciculus (Forkel et al., 2014). Regarding cerebellar activation, one might hypothesize that in the absence of proprioception the brain attempts to compensate by rescuing motor programs and visual imagery stored in the cerebellum (Baumann et al., 2015; Kansal et al., 2017).

Perruchoud et al. (2014) proposes that, for each fraction of a

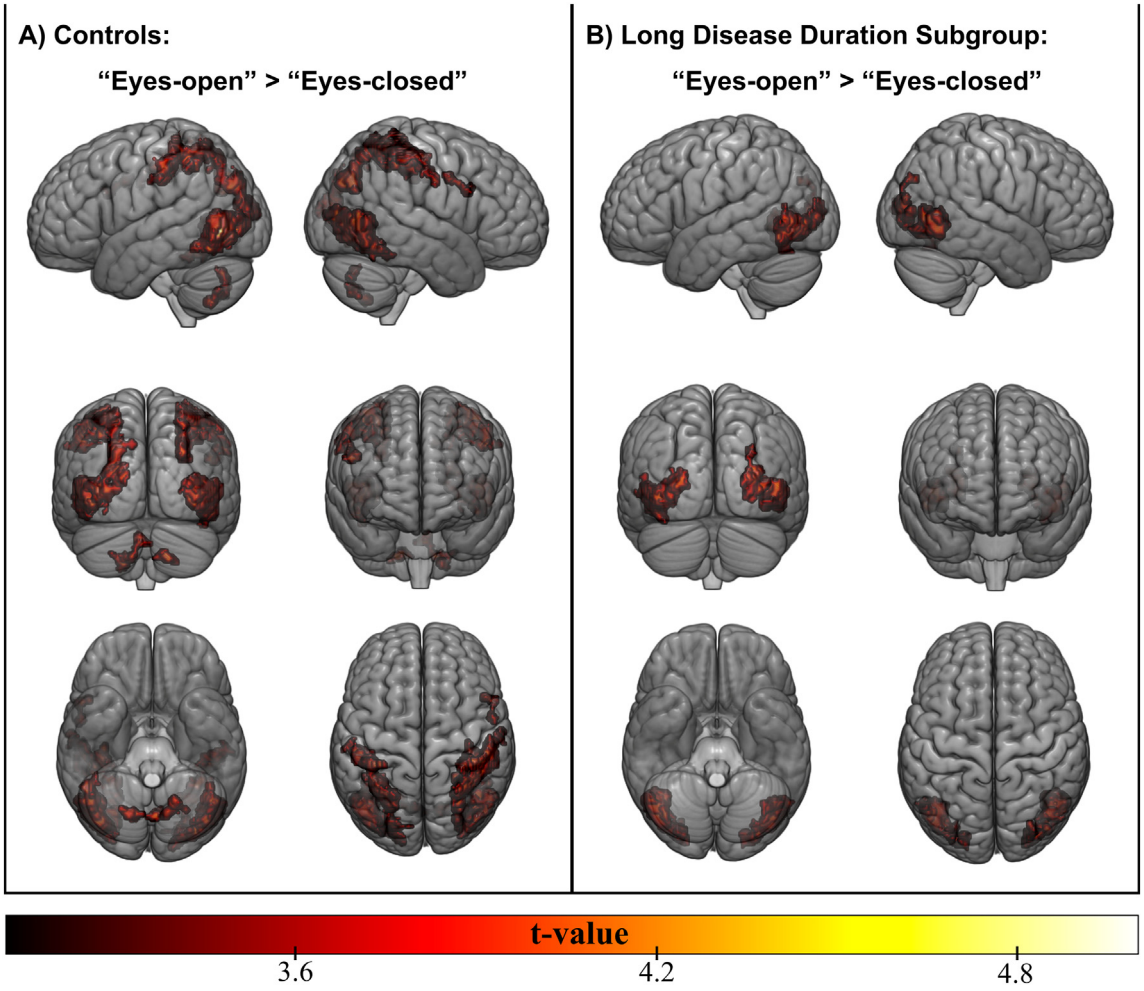

Fig. 5. Activation maps related to the finger-tapping task. Greater activation during eyes-open compared to eyes-closed condition is shown for (A) controls and (B) long disease duration subgroup of SN patients.

movement, brain motor areas generate an efference plan, which commands body muscles, and also an "efference [plan] copy" used to predict the sensory outcome of the intended movement. While the movement is executed, this sensory prediction is compared to the real sensory information provided by body receptors, and the error between them is forwarded to sensory and secondary motor areas. These areas would finally calibrate the efference plan and the efference copy, completing the cycle. Authors also suggest that the parietal cortex receives the efference copy and sensory information (body current state) to generate the expected sensory outcome, and passes it on to the cerebellum. The cerebellum receives both this prediction and the actual sensory information, communicating the two (predicted and measured) to the basal ganglia and the thalamus. Together, these three structures (cerebellum, basal ganglia and thalamus) would estimate the sensory error and inform the primary sensory cortex and the secondary motor areas, responsible to (re)calibrate efference plan and deliver it to the primary motor area. In the pathological scenario of our patients, there is probably a mismatch between the predicted and the measured sensory information, since the actual state of the body is defectively measured.

Taking into account results of task-fMRI experiments, we specifically found that the paramedian cerebellum was not activated in the SN group (nor was there any major difference between the visually and non-visually guided activation maps), and interestingly this region closely matches the classical cerebellar sensorimotor integration areas (Grodd et al., 2001; Bostan et al., 2013). In the absence of sensory input, the cerebellum is thus under-activated emulating clinical signs of ataxia, even without structural cerebellar damage. A similar explanation might account for the lack of parietal activation in the SN group. We hypothesize that in the absence of sensory input, posterior parietal cortex cannot properly integrate other afferent inputs (e.g., vision) and, therefore, remains silent.

Cerebellar and parietal findings corroborates Perruchoud et al.'s model (Perruchoud et al., 2014), since the "sensory inflow" to the cerebellum is defective, as well as the sensory error that is informed to the parietal region. However, the abnormal hypertrophy of caudate nuclei may indicate a possible update to the model, highlighting caudate role in the integration of sensory and motor information (perhaps the error estimation between the predicted with the real sensory information).

5. Conclusion

Overall, our results seem to indicate a disruption of the basal ganglia communication, at least in a structural level. We also highlight that WM and GM regions identified in this study are critically related to the sensory-motor circuitry, since the thalamus is a relay of sensory information and some of the tracts affected (mainly corona radiata and internal capsule) are intimately related to its function and also to striatum activity. This may reflect a compensatory adaptation due to neuronal plasticity, not necessarily benign, since impairment progresses along with the disease. Finally, task-related results pointed to a difference in cerebral activation as a consequence of lack of input, specifically in the posterior parietal regions and in medial areas of the

cerebellar lobes (VIII and VI).

Considering practical purposes, the present study identified the brain regions and systems affected by the lack on somatosensory feedback as a consequence of a movement. Thus, it could be suggested that future rehabilitation programs might benefit from the inclusion of experimental tasks able to increase the activity of the regions reported here (posterior parietal cortex and cerebellum) and/or neurostimulation techniques for focused enhancement of baseline neural firing (e.g. transcranial direct (or alternating) current stimulation or transcranial magnetic stimulation). The compensation of brain deficits identified in our investigation, might result in a better balance between motor output and sensory input, aiming to restore proper sensorimotor loop. Hence, the present study could constitute an important reference for future development of rehabilitation strategies.

Declarations of interest

None.

Funding

This study was supported by São Paulo Research Foundation (FAPESP) [grants numbers 2013/01766-7 and 2014/15918-6].

References

Araneda, R., Renier, L.A., Rombaux, P., Cuevas, I., De Volder, A.G., 2016. Cortical plasticity and olfactory function in early blindness. Front. Syst. Neurosci. 10, 75. https://doi.org/10.3389/fnsys.2016.00075.

Ashburner, J., Friston, K.J., 2005. Unified segmentation. NeuroImage 26, 839–851. https://doi.org/10.1016/j.neuroimage.2005.02.018.

Baumann, O., Borra, R.J., Bower, J.M., Cullen, K.E., Habas, C., Ivry, R.B., Leggio, M., Mattingley, J.B., Molinari, M., Moulton, E.A., Paulin, M.G., Pavlova, M.A., Schmahmann, J.D., Sokolov, A.A., 2015. Consensus paper: the role of the cerebellum in perceptual processes. Cerebellum 14, 197–220. https://doi.org/10.1007/s12311-014-0627-7.

Benjamini, Y., Hochberg, Y., 1995. Controlling the false discovery rate – a practical and powerful approach to multiple testing. J. R. Stat. Soc. Ser. B Methodol. 57, 289–300. https://doi.org/10.2307/2346101.

Bostan, A.C., Dum, R.P., Strick, P.L., 2013. Cerebellar networks with the cerebral cortex and basal ganglia. Trends Cogn. Sci. 17, 241–254. https://doi.org/10.1016/j.tics.2013.03.003.

Camdessanché, J.-P., Jousserand, G., Ferraud, K., Vial, C., Petiot, P., Honnorat, J., Antoine, J.-C., 2009. The pattern and diagnostic criteria of sensory neuronopathy: a case-control study. Brain 132, 1723–1733. https://doi.org/10.1093/brain/awp136.

Casseb, R.F., Martinez, A.R.M., de Paiva, J.L.R., França, M.C., 2015. Neuroimaging in sensory neuronopathy. J. Neuroimaging 25, 704–709. https://doi.org/10.1111/jon.12210.

Choe, A.S., Belegu, V., Yoshida, S., Joel, S., Sadowsky, C.L., Smith, S.A., van Zijl, P.C.M., Pekar, J.J., McDonald, J.W., 2013. Extensive neurological recovery from a complete spinal cord injury: a case report and hypothesis on the role of cortical plasticity. Front. Hum. Neurosci. 7, 290. https://doi.org/10.3389/fnhum.2013.00290.

Cotman, C.W., Matthews, D.A., Taylor, D., Lynch, G., 1973. Synaptic rearrangement in the dentate gyrus: histochemical evidence of adjustments after lesions in immature and adult rats. Proc. Natl. Acad. Sci. U. S. A. 70, 3473–3477.

de Campos, B.M., Coan, A.C., Lin Yasuda, C., Casseb, R.F., Cendes, F., 2016. Large-scale brain networks are distinctly affected in right and left mesial temporal lobe epilepsy. Hum. Brain Mapp. 37, 3137–3152. https://doi.org/10.1002/hbm.23231.

Eklund, A., Nichols, T.E., Knutsson, H., 2016. Cluster failure: why fMRI inferences for spatial extent have inflated false-positive rates. Proc. Natl. Acad. Sci. U. S. A. 113, 7900–7905. https://doi.org/10.1073/pnas.1602413113.

Endo, T., Spenger, C., Tominaga, T., Brene, S., Olson, L., 2007. Cortical sensory map rearrangement after spinal cord injury: fMRI responses linked to Nogo signalling. Brain 130, 2951–2961. https://doi.org/10.1093/brain/awm237.

Fischl, B., 2012. FreeSurfer. NeuroImage 62, 774–781. https://doi.org/10.1016/j.neuroimage.2012.01.021.

Forkel, S.J., Thiebaut de Schotten, M., Kawadler, J.M., Dell'Acqua, F., Danek, A., Catani, M., 2014. The anatomy of fronto-occipital connections from early blunt dissections to contemporary tractography. Cortex 56, 73–84. https://doi.org/10.1016/j.cortex.2012.09.005.

Gooijers, J., Swinnen, S.P., 2014. Interactions between brain structure and behavior: the corpus callosum and bimanual coordination. Neurosci. Biobehav. Rev. 43, 1–19.

Goyal, M., Versnick, E., Tuite, P., Cyr, J. Saint, Kucharczyk, W., Montanera, W., Willinsky, R., Mikulis, D., 2000. Hypertrophic olivary degeneration: metaanalysis of the temporal evolution of MR findings. AJNR Am. J. Neuroradiol. 21, 1073–1077.

Grodd, W., Hülsmann, E., Lotze, M., Wildgruber, D., Erb, M., 2001. Sensorimotor mapping of the human cerebellum: fMRI evidence of somatotopic organization. Hum. Brain Mapp. 13, 55–73. https://doi.org/10.1002/hbm.1025.

Horta, C.A., Silva, F.V.G., Moraes, A., Pradella, F., Paula, R., Ramos, V., Oliveira, E., Brandao, C.O., Jr, M.C.F., Longhini, A.L., Farias, A., Santos, L.M.B., Nucci, A., 2011. Profile of inflammatory cells in the CSF and peripheral blood, expression of IL-17 and IL-27 and T cells mediated response in untreated patients with idiopathic gangliopathy. Neurology 76, A464.

Kansal, K., Yang, Z., Fishman, A.M., Sair, H.I., Ying, S.H., Jedynak, B.M., Prince, J.L., Onyike, C.U., 2017. Structural cerebellar correlates of cognitive and motor dysfunctions in cerebellar degeneration. Brain 127, aww327. https://doi.org/10.1093/brain/aww327.

Lewis, T.L., Maurer, D., 2005. Multiple sensitive periods in human visual development: evidence from visually deprived children. Dev. Psychobiol. 46, 163–183. https://doi.org/10.1002/dev.20055.

Li, Y., Shea, S.M., Lorenz, C.H., Jiang, H., Chou, M.-C., Mori, S., 2013. Image corruption detection in diffusion tensor imaging for post-processing and real-time monitoring. PLoS One 8, e49764. https://doi.org/10.1371/journal.pone.0049764.

Makin, T.R., Scholz, J., Henderson Slater, D., Johansen-Berg, H., Tracey, I., 2015. Reassessing cortical reorganization in the primary sensorimotor cortex following arm amputation. Brain 138, 2140–2146. https://doi.org/10.1093/brain/awv161.

Martins Rosa, A., Silva, M.F., Ferreira, S., Murta, J., Castelo-Branco, M., Murta, J., Castelo-Branco, M., 2013. Plasticity in the human visual cortex: an ophthalmology-based perspective. Biomed. Res. Int. 2013, 568354. https://doi.org/10.1155/2013/568354.

Mori, S., Wu, D., Ceritoglu, C., Li, Y., Kolasny, A., Vaillant, M.A., Faria, A.V., Oishi, K., Miller, M.I., 2016. MRICloud: delivering high-throughput MRI neuroinformatics as cloud-based software as a service. Comput. Sci. Eng. 18, 21–35. https://doi.org/10.1109/MCSE.2016.93.

Okumura, R., Asato, R., Shimada, T., Kusaka, H., Mizutani, T., Miki, Y., Konishi, J., 1992. Degeneration of the posterior columns of the spinal cord: postmortem MRI and histopathology. J. Comput. Assist. Tomogr. 16, 865–867.

Patel, N., Hanfelt, J., Marsh, L., Jankovic, J., members of the Dystonia Coalition, 2014a. Alleviating manoeuvres (sensory tricks) in cervical dystonia. J. Neurol. Neurosurg. Psychiatry 85, 882–884. https://doi.org/10.1136/jnnp-2013-307316.

Patel, N., Jankovic, J., Hallett, M., 2014b. Sensory aspects of movement disorders. Lancet Neurol. 13, 100–112. https://doi.org/10.1016/S1474-4422(13)70213-8.

Perruchoud, D., Murray, M.M., Lefebvre, J., Ionta, S., 2014. Focal dystonia and the Sensory-Motor Integrative Loop for Enacting (SMILE). Front. Hum. Neurosci. 8, 458. https://doi.org/10.3389/fnhum.2014.00458.

Raffin, E., Richard, N., Giraux, P., Reilly, K.T., 2016. Primary motor cortex changes after amputation correlate with phantom limb pain and the ability to move the phantom limb. NeuroImage 130, 134–144. https://doi.org/10.1016/j.neuroimage.2016.01.063.

Raisman, G., 1969. Neuronal plasticity in the septal nuclei of the adult rat. Brain Res. 14, 25–48.

Rezende, T.J.R., Silva, C.B., Yassuda, C.L., Campos, B.M., D'Abreu, A., Cendes, F., Lopes-Cendes, I., França, M.C., 2016. Longitudinal magnetic resonance imaging study shows progressive pyramidal and callosal damage in Friedreich's ataxia. Mov. Disord. 31, 70–78. https://doi.org/10.1002/mds.26436.

Schmitz-Hübsch, T., du Montcel, S.T., Baliko, L., Berciano, J., Boesch, S., Depondt, C., Giunti, P., Globas, C., Infante, J., Kang, J.-S., Kremer, B., Mariotti, C., Melegh, B., Pandolfo, M., Rakowicz, M., Ribai, P., Rola, R., Schöls, L., Szymanski, S., van de Warrenburg, B.P., Dürr, A., Klockgether, T., Fancellu, R., 2006. Scale for the assessment and rating of ataxia: development of a new clinical scale. Neurology 66, 1717–1720. https://doi.org/10.1212/01.wnl.0000219042.60538.92.

Simoes, E.L., Bramati, I., Rodrigues, E., Franzoi, A., Moll, J., Lent, R., Tovar-Moll, F., 2012. Functional expansion of sensorimotor representation and structural reorganization of callosal connections in lower limb amputees. J. Neurosci. 32, 3211–3220. https://doi.org/10.1523/jneurosci.4592-11.2012.

Tang, X., Oishi, K., Faria, A.V., Hillis, A.E., Albert, M.S., Mori, S., Miller, M.I., 2013. Bayesian parameter estimation and segmentation in the multi-atlas random orbit model. PLoS One 8, e65591. https://doi.org/10.1371/journal.pone.0065591.

Tang, X., Yoshida, S., Hsu, J., Huisman, T.A.G.M., Faria, A.V., Oishi, K., Kutten, K., Poretti, A., Li, Y., Miller, M.I., Mori, S., 2014. Multi-contrast multi-atlas parcellation of diffusion tensor imaging of the human brain. PLoS One 9, e96985. https://doi.org/10.1371/journal.pone.0096985.

Tang, X., Crocetti, D., Kutten, K., Ceritoglu, C., Albert, M.S., Mori, S., Mostofsky, S.H., Miller, M.I., 2015. Segmentation of brain magnetic resonance images based on multi-atlas likelihood fusion: testing using data with a broad range of anatomical and photometric profiles. Front. Neurosci. 9, 61. https://doi.org/10.3389/fnins.2015.00061.

Tustison, N.J., Avants, B.B., Cook, P.A., Yuanjie Zheng, Y., Egan, A., Yushkevich, P.A., Gee, J.C., 2010. N4ITK: improved N3 bias correction. IEEE Trans. Med. Imaging 29, 1310–1320. https://doi.org/10.1109/TMI.2010.2046908.

Voss, P., Zatorre, R.J., 2015. Early visual deprivation changes cortical anatomical covariance in dorsal-stream structures. NeuroImage 108, 194–202. https://doi.org/10.1016/j.neuroimage.2014.12.063.

Wang, H., Pouch, A., Takabe, M., Jackson, B., Gorman, J., Gorman, R., Yushkevich, P.A., 2013. Multi-atlas segmentation with robust label transfer and label fusion. Inf. Process. Med. Imaging 23, 548–559.

Woods, R.P., Grafton, S.T., Holmes, C.J., Cherry, S.R., Mazziotta, J.C., 1998. Automated image registration: I. General methods and intrasubject, intramodality validation. J. Comput. Assist. Tomogr. 22, 139–152. https://doi.org/10.1097/00004728-199801000-00027.

Wu, D., Ma, T., Ceritoglu, C., Li, Y., Chotiyanonta, J., Hou, Z., Hsu, J., Xu, X., Brown, T., Miller, M.I., Mori, S., 2016. Resource atlases for multi-atlas brain segmentations with multiple ontology levels based on T1-weighted MRI. NeuroImage 125, 120–130. https://doi.org/10.1016/j.neuroimage.2015.10.042.

Zhuang, J., Hrabe, J., Kangarlu, A., Xu, D., Bansal, R., Branch, C.A., Peterson, B.S., 2006. Correction of eddy-current distortions in diffusion tensor images using the known directions and strengths of diffusion gradients. J. Magn. Reson. Imaging 24, 1188–1193. https://doi.org/10.1002/jmri.20727.